Investigating the Role of Wave-like Reflectivity Segments during the 17 November 2013 EF-4 Washington, Illinois Tornado

Ed Shimon*
National Weather Service
Central Illinois, Lincoln IL

1. INTRODUCTION

Early investigations into the interactions of atmospheric waves with convection focused mainly on convective initiation or convective enhancement. (e.g., Uccellini 1975; Stobie et al. 1983; Koch et al. 1988; Schmidt and Cotton 1990; Corfidi 1998). Other work evolved into the study of atmospheric waves interaction with mesocyclones and tornadoes (e.g., Miller and Sanders 1980; Kilduff 1999; Barker 2006). Barker (2006) found a link between "reflectivity tags" (which were assumed to be waves) that moved quickly through linear convection and were associated with tornadogenesis.

Colman and Knupp (2008) utilized a simple model and observations to show how the interaction of ducted gravity waves with a mesocyclone could increase the vertical vorticity (ζ) of the low-level mesocyclone. They showed that the ζ increase occurred through low-level vorticity stretching due to convergence ahead of wave ridges and/or the tilting of horizontal vorticity into the vertical associated with perturbation wind shear in the wave ridges (figures 1 and 2).

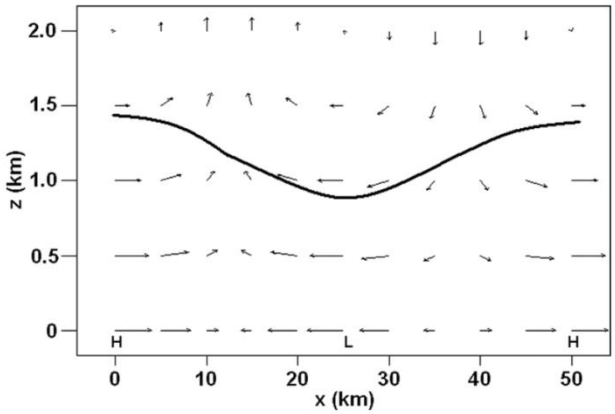

Figure 1 - Airflow vectors and an isentrope (heavy solid curve) in the x-z plane for a ducted gravity wave with a wave duct just above 2 km. Divergence is largest near the surface, with convergence located ahead of a wave ridge and divergence ahead of a wave trough. Positive perturbation wind shear is centered in the wave trough and negative shear centered in the ridge. Coleman and Knupp (2008)

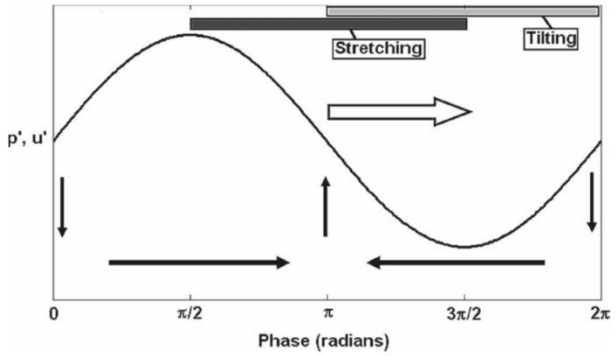

Figure 2 - Regions of expected positive wave-induced stretching and tilting through interaction with a mesocyclone, relative to the gravity wave phase. Coleman and Knupp (2008)

*Corresponding author address: Ed Shimon NOAA/NWS 1362 State Route 10 Lincoln, IL 62656 e-mail: edward.shimon@noaa.gov

The views expressed are those of the author and do not necessarily represent those of the National Weather Service.

Murphy et al. (2014) have done the first in-depth kinematic analysis of wave-like reflectivity segment (WRS) interaction with mesocyclones. Their major findings included the presence of enhanced horizontal vorticity within the WRSs, which trajectory analyses indicated entered the convective core of the QLCS during interaction, subsequently followed by an increase in the vertical vorticity of the convective core, and lead to tornadogenesis. They defined a WRS as:

- An area of weak-to-moderate radar reflectivity (between 10 and 40-45 dBZ)
- Major axis dimension much greater than minor axis (i.e., linear radar appearance; typically, but not always, oriented in east-west direction)
- Moving faster than component of the background wind in their direction of motion (i.e., exhibits propagation in addition to advection)
- Exhibits significant pressure perturbations ($\geq$ 0.5-1.0hPa) at the surface.

Murphy and Knupp (2014) have studied the frequency of tornadoes correlated with WRSs in the 2005-2012 years across the Tennessee Valley. They found that WRSs occurred on roughly two-thirds of the tornado days. Of all 236 tornadoes in their study, 23% were spatially and temporally correlated with a WRS-convection interaction.

So clearly, interactions of WRSs with convection appear to be a relatively common feature in severe weather environments. On 17 November 2013, a violent cold-season tornado devastated the community of Washington, Illinois, producing widespread EF-4 damage. During post-event analysis, two WRSs were identified moving through the near-storm environment during critical times of the parent supercell's life cycle. This study will focus on what role those WRSs may have played in tornadogenesis and the subsequent production of EF-4 damage.

2. OBSERVATIONAL ANALYSIS

2.1 Synoptic and Mesoscale Environment

The synoptic and mesoscale environment over central Illinois on 17 November 2013 was extremely conducive to severe weather, as evidenced by the High Risk Day One Outlook including central and eastern Illinois (figure 3). Storm Prediction Center (SPC) noted the potential for several long-track violent EF-2 to EF-5 tornadoes that day in the High Risk area.

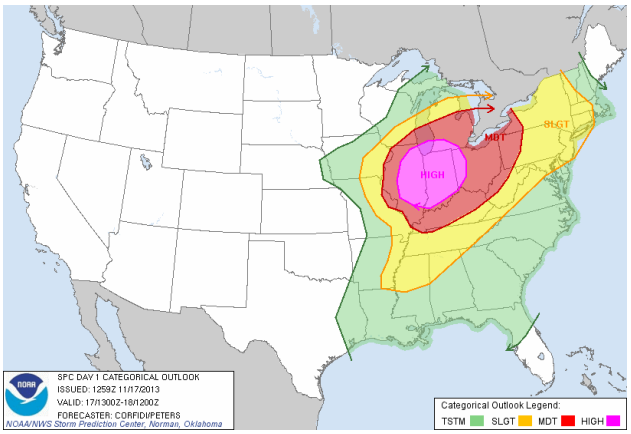

Figure 3 – SPC Day 1 Outlook, 1300 UTC, 17 Nov 2013.

By 1600 UTC that morning, an impressive negatively-tilted 300-hPa trough extended from the Dakotas into Missouri. A powerful 100-110 kt 300-hPa jet was rounding the base of the trough from Nebraska into west-central Illinois. A 65-70 kt 850-hPa jet extended from southeastern Missouri into northeastern Illinois. At the surface, a 991-hPa pressure minimum was moving from northern Missouri at 1200 UTC to northern Illinois at 1600 UTC with a cold front trailing to the south of the low into western Illinois. Strong moisture advection ahead of the front was fueled by the low-level

jet, as highly anomalous surface dewpoints for mid-November climbed into the low to mid 60s °F in central Illinois by 1600 UTC.

The 1600 UTC Lincoln, Illinois (KILX) sounding (figure 4) confirmed that the instability and shear parameters matched closely to what Murphy et al. (2014), Barker (2006) and Chadwick (1998) had discovered as typical environments for WRS days. Murphy et al. (2013) and Barker (2006) found that the environments that appeared to be most conducive for WRS interaction were highly dynamic, and contained low convective available potential energy (CAPE) and relatively high shear. Some corresponding calculations from the 16 UTC KILX sounding were:

- mixed-layer CAPE - 1313 Jkg^{-1}
- 0-1km shear - 19 ms^{-1} (37 kts),
- 0-6km shear - 37 ms^{-1} (71 kts)
- 0-1km storm-relative helicity - 318 m^2s^{-2}

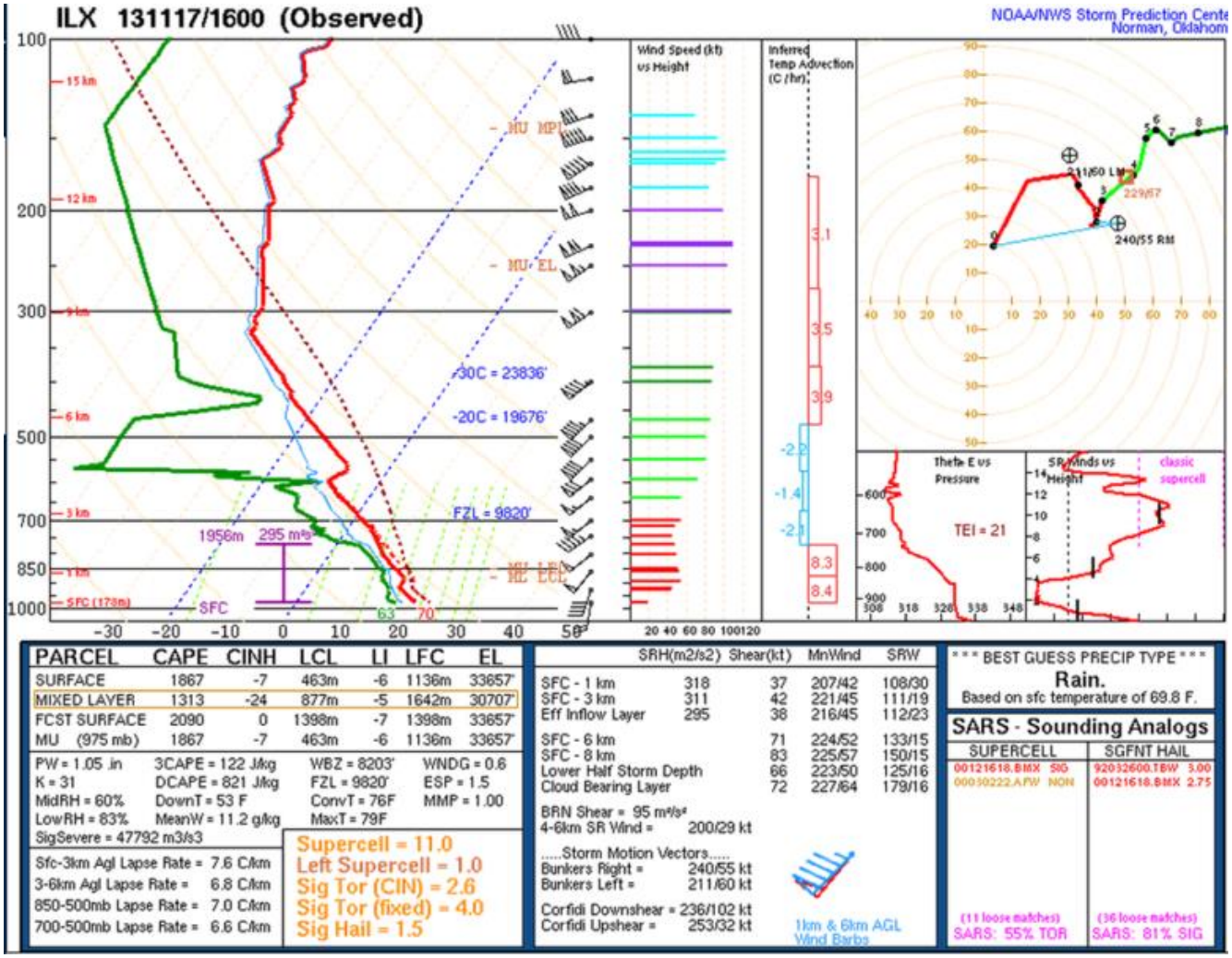

Figure 4 – KILX 1600 UTC Sounding, 17 Nov 2013.

Chadwick (1998) found that wave segments often appeared to be linked to a jet streak evident in GOES 6.7 µm imagery (figure 5). KILX WSR-88D VAD wind profiler data (figure 6) from the time of the tornado also confirmed the presence of a 56 ms^{-1} (109 kt) jet passing above the tornadic supercell during the time it struck Washington, Illinois.

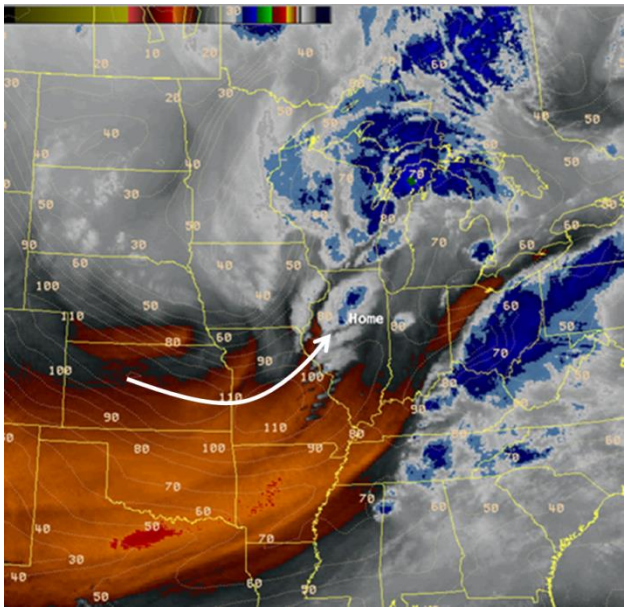

Figure 5 - GOES 6.7 µm image and RUC 400-hPa 0-hr wind speed (dotted tan – 10-kt contour interval) 1600 UTC 17 Nov 2013. "Home" marks Washington, Illinois.

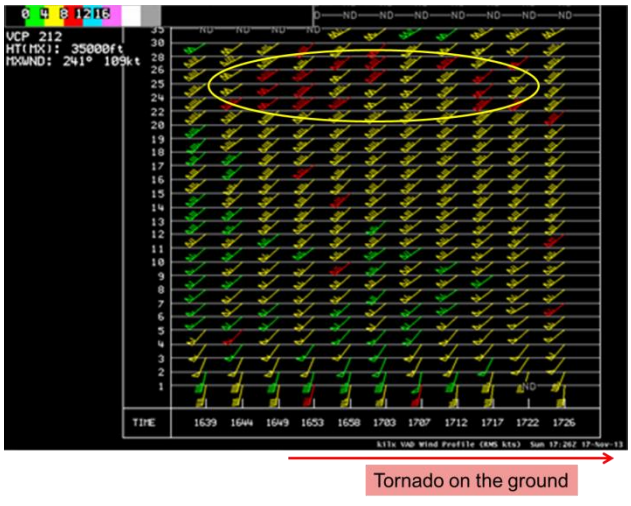

Figure 6 – KILX VAD wind profile – 1639 UTC to 1726 UTC.

2.2 Radar Analysis

During post-event analysis, there appeared to be evidence of two WRSs interacting with the parent supercell to possibly alter the near-storm environment in favor or tornadogenesis and/or meso-cyclone intensification. It is hypothesized that the first WRS (WRS1) played a role in triggering tornadogenesis while the second WRS (WRS2) may have triggered an abrupt intensification of the tornado just prior to it producing EF-4 damage across Washington, Illinois, which was the only period of EF-4 damage that it produced during its life cycle.

The WRSs were not readily apparent in the KILX WSR-88D 0.5° elevation reflectivity (Z) and velocity (V) data until a fast-loop methodology was employed (Barker 2006). Also, the WRSs were only visible in the 0.5° Z and V data for a few volume scans before they passed or merged with the parent supercell. A 4-panel of four low elevation slices of Z (0.5°, 1.3°, 2.4°, 3.1°) gave an earlier view of the WRSs, and allowed for continued use of the fast-loop methodology. Once the WRSs were identified, the most effective method of identifying their full spatial extent was to utilize the Four-dimension Stormcell Investigator (FSI) application, available in the Advanced Weather Interactive Processing System (AWIPS). While fast-looping is not an available function in FSI, it still gives a much more thorough analysis of the horizontal and vertical reflectivity profiles.

Utilizing 0.5° Z KILX data, WRS1 first became evident at 1630 UTC. The 2.4° Z elevation showed WRS1 as early as 1620 UTC. Its forward progress was tracked at 36 ms^{-1} (70 kts), while the supercell speed was 27 ms^{-1} (52 kts. As previously indicated, FSI gave a more thorough picture of the WRSs (figure 7), and FSI images will be used to discuss the progression of the WRSs.

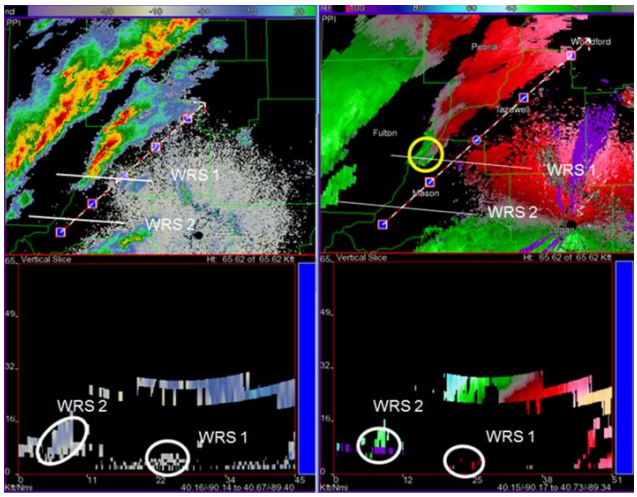

Figure 7 – FSI images of KILX Z (left half) and V (right half) at 1630 UTC Nov 17, 2013. Top images are 0.5° Z and V, while the bottom images are vertical cross sections along the SW-NE-oriented cross-section line displayed in top images. White circles in the bottom images show the location of the WRSs. The yellow circle in the upper left highlights the mesocyclone in the supercell.

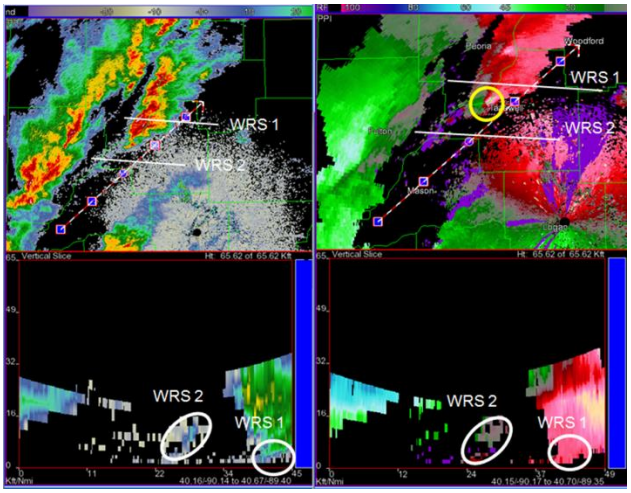

Figure 8 – Same as Figure 7 except 1649 UTC

Figure 8 visually shows the enhancement that occurred in the mesocyclone at 1649 UTC, which was about 10 minutes after WRS1 passed through the supercell.

Figure 9 shows a quantitative time-progression analysis of the rotational velocity with height and distance from the KILX radar.

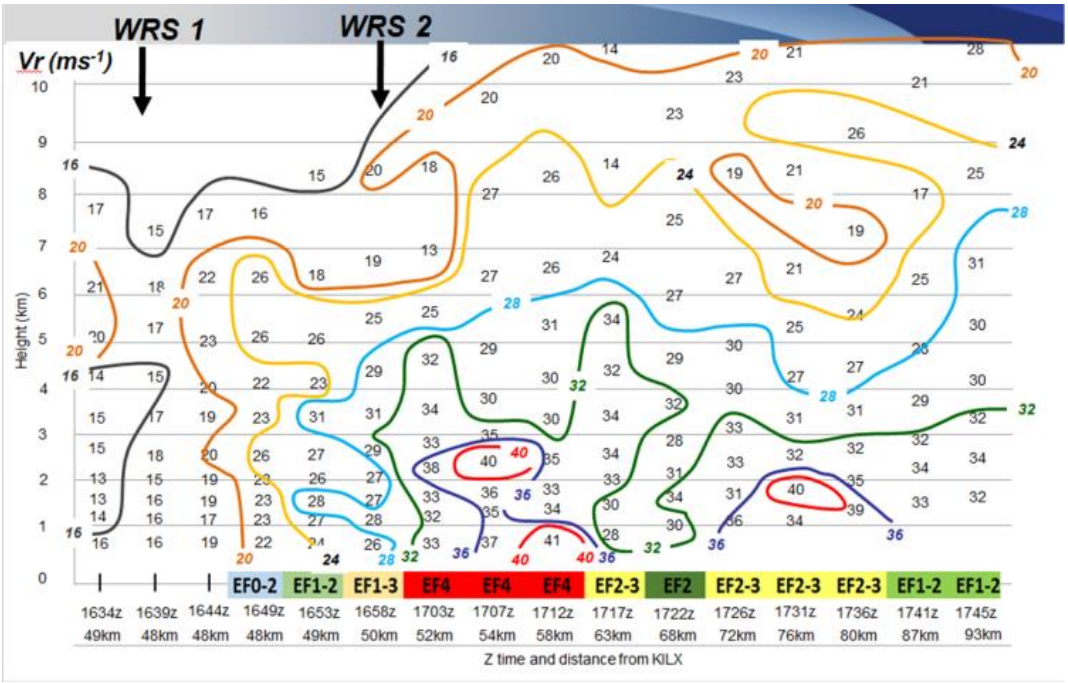

Figure 9 – Rotational velocity diagram (ms^{-1}). Colored lines show rotational velocity in increments of 4 ms^{-1}. Increasing height (km) on left side. Across bottom: Increasing time by volume scan, EF rating of tornado, and distance from the KILX radar. Time of interaction with WRS1 and WRS2 indicated by the black arrows at the top of the diagram.

Descending intensification of the meso-cyclone began immediately after interaction with WRS1 at 1639 UTC, with tornadogenesis delayed by around 10 minutes. The tornado produced mainly EF-0 and EF-1 damage until the intersection of WRS2 with the tornadic mesocyclone around 1658 UTC. Figure 9 shows the immediate quantitative intensification of the rotational velocities below 5 km, with more dramatic intensification below 3 km. Figures 10, 11 and 12 show the qualitative increase in rotation in the KILX V at 0.5°.

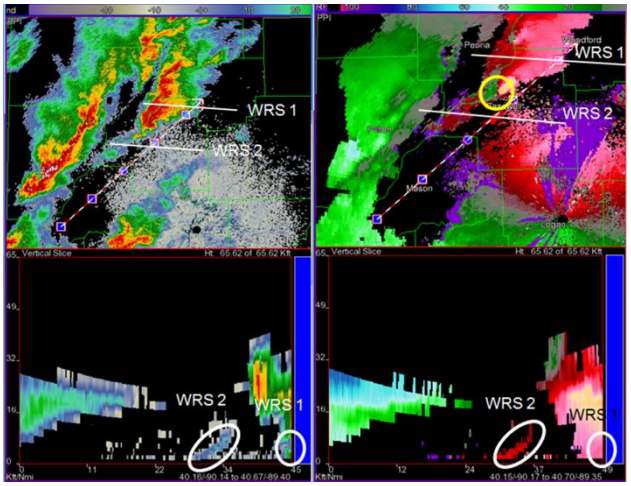

Figure 10 – Same as Figure 7 except 1653 UTC

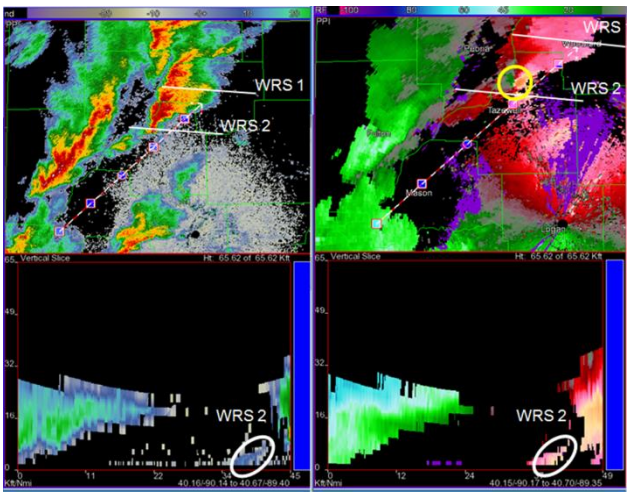

Figure 11 – Same as Figure 7 except 1658 UTC

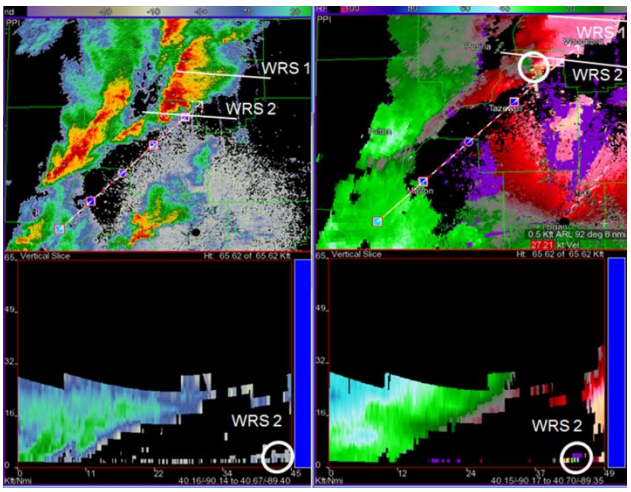

Figure 12 – Same as Figure 7 except 1703 UTC

There is also direct video evidence of the evolution of the tornado funnel during the period of time surrounding the intersection of WRS2 and the tornadic supercell as documented in Figures 13 through 16. The video clip snapshots in Figures 14 and 16 specifically show the dramatic visual intensification of the tornado circulation as it went from a barely visible condensation funnel around 1659 UTC to a 500-meter (0.3 mile) wide tornado producing EF-4 damage by 1704 UTC.

This study did not have access to an intricate observation network such as the one used by Murphy et al. (2013) to do a quantitative analysis of low-level vorticity tilting and stretching. However, there is compelling video evidence of dramatic tornado intensification from before and after WRS2 intersected the tornado circulation.

The tornado went on to produce EF-4 damage for the next 9 minutes as it devastated Washington, Illinois. Figure 9 shows the weakening of the rotational velocities below 3 km and lower EF damage at 1717 and 1722 UTC as the tornado departed farther from Washington, Illinois. No additional EF-4 damage occurred from that tornado even though

it struck several other communities after passing through open farmland.

Figure 13 – Google map showing position of videographer, Clint Plunk, on the west side of Washington, Illinois, (yellow circle) looking to the SW (yellow arrow) at 1659 UTC. Red plot is the damage path width.

Figure 14 – Snapshot from Clint Plunk video of the tornado near Farmdale Park to the SW of Washington, Illinois at 1659 UTC.

One additional item of note with respect to the evolution of WRS2 was that it descended with height in the last three volume scans before intersecting with the tornadic supercell. (Figures 8, 10-12). That tendency had not been documented in previous WRS research that this author reviewed.

Figure 15 – Google map showing position of videographer (anonymous) on the west side of Washington, Illinois, (yellow circle) looking to the SSE (yellow arrow) at 1704 UTC. Red plot is the damage path width.

Figure 16 – Snapshot from anonymous video of the tornado near SW side of Washington, Illinois at 1704 UTC.

Throughout the descent, the WRS seemed to maintain the 2-3-km height, which is a typical depth for a WRS (Murphy et al. 2014). The exact cause of the descent by the WRS is not known, but it may have been part of the reason why the low-level tornadic circulation intensified so rapidly. A simple hypothesis may be related to the wave being affected by descending air in the rear-flank downdraft, but

no direct evidence is available to support that with this case.

3. DISCUSSION AND CONCLUSIONS

The synoptic and mesoscale environment in this case fit the template for WRS days as noted by Murphy et al. (2014), Barker (2006) and Chadwick (1998). The low CAPE, high shear, and jet streak interaction were all present. Murphy and Knupp (2014) had linked WRS days with a low Bulk Richardson Number (BRN ~ 1.4) and Richardson number (Ri < 0.25), but those data were not documented for this case and could be a focus for future study. The significance of the low Richardson number is its evidence of low-level Kelvin-Helmholtz instability in the layer the waves may be traveling, which is a favorable environment for gravity wave propagation. (Murphy and Knupp 2014).

The identification of WRSs in the operational setting utilizing WSR-88D data still remains a challenge due to weaker scattered convection that can surround ongoing organized intense convection. A combination of analyzing radar fast-loops of Z, V, and SRM data combined with FSI cross-sectional analysis may be a more effective methodology to quickly identify WRSs in real time.

There is supporting evidence from analysis of meteorological and radar data as well as video documentation in this case that the intersection of WRSs with the parent supercell appears to have played a role in both tornadogenesis and in the rapid intensification of the tornado. Although the exact cause of the waves and classification of the waves as gravity waves has not been determined by the evidence in this case, one goal of the study was to enhance our understanding of how to utilize the qualitative evidence readily available to forecasters during severe weather operations. The intended result would be to improve warning lead time and accuracy in support of the National Weather Service mission of saving lives and property.

4. ACKNOWLEDGEMENTS

The author would like to express his appreciation to Todd Murphy from the University of Alabama Huntsville for background discussions on his quantitative research into WRSs. The author would like to thank Dan Miller, SOO NOAA/NWS Duluth MN for his discussions on low-level thermodynamics and shear profiles on significant tornado days. The author would also like to thank Llyle Barker, SOO, NWS Lincoln, Illinois for his help in reviewing this document, and acknowledge Ernest Goetsch, MIC, NWS Lincoln, Illinois for his support of this research endeavor.

5. REFERENCES

Barker, L. J., 2006: A Potentially Valuable WSR-88D Severe Storm Pre-cursor Signature in Highly Dynamic, Low Cape, High Shear Environments. Preprints, 23rd Conf. on Severe Local Storms, St. Louis, MO, Amer. Meteor. Soc.

Browning, K. A., 1971: Structure of the atmosphere in the vicinity of large amplitude Kelvin Helmholtz billows. Quart. J. Roy. Meteor. Soc., **97**, 283-299.

Chimonas, G., and J. R. Grant, 1984: Shear Excitation of Gravity Waves. Part II: Upscale Scattering from Kelvin-Helmholtz Waves. J. Atmos. Sci., **41**, 2278–2288.

Coleman T., and K. Knupp, 2006: The interaction of gravity waves with tornadoes and mesocyclones: Theories and observations. Preprints, 23rd Conference on Severe Local Storms, Saint Louis, MO, Amer. Meteor. Soc.

Coleman, T. A., and K. R. Knupp, 2008: The Interactions of Gravity Waves with Mesocyclones: Preliminary Observations and Theory. *Mon. Wea. Rev*., **136**, 4206–4219.

Chadwick, R.B., 1988: The Wind Profiler Demonstration Network. Extended Abstracts, Symp. on Lower Tropospheric Profiling: Needs and Technologies, Boulder, CO, Amer. Meteor. Soc.

Corfidi, S. F., 1998: Some thoughts on the role mesoscale features played in the 27 May 1997 central Texas tornado outbreak. Preprints, *19th Conf. on Severe Local Storms*, Minneapolis, MN, Amer. Meteor. Soc.

Crum, T., and R. Alberty, 1993: The WSR-88D and the WSR-88D Operational Support Facility. Bull. Amer. Meteor. Soc., 74, 1669-1687.

Jewett B., R. Rauber, and G. McFarquhar, 2003: Large amplitude mesoscale gravity waves: New studies of their formation and evolution. Preprints, Midwest Extreme and Hazardous Weather Conference, Champaign, IL, Amer. Meteor. Soc.

Kilduff, R. E., 1999: The interaction of a gravity wave with a thunderstorm. Electronic poster, NOAA/National Weather Service.

Koch, S. E., and P. B. Dorian, 1988: A mesoscale gravity wave event observed during CCOPE. Part III: Wave environment and source mechanisms. *Mon. Wea. Rev.,* **116,** 2570–2592.

Koch, S. E., and R. E. Golus, 1988: A Mesoscale Gravity Wave Event Observed during CCOPE. Part I: Multiscale Statistical Analysis of Wave Characteristics. *Mon. Wea. Rev.*, **116**, 2527–2544.

Koch, S. E., and C. O'Handley, 1997: Operational forecasting and detection of mesoscale gravity waves. *Wea. Forecasting*, **12,** 253–281.

Koch, S. E., R. E. Golus, and P. B. Dorian, 1988: A mesoscale gravity wave event observed during CCOPE. Part II: Interactions between mesoscale convective systems and the antecedent waves. *Mon. Wea. Rev.*, **116,** 2545–2569.

Koch, S., F. Einaudi, P. Dorian, S. Lang, G. Heymsfield, 1993: Mesoscale gravity-wave event observed during CCOPE. Part IV: stability analysis and doppler-derived wave vertical structure, Mon. Wea. Rev., **121**, 2483-2510.

Koch, S. and S. Saleeby, 2001: An automated system for the analysis of gravity waves and other mesoscale phenomena, Wea. Forecasting, **16**, 661-679.

MacDonald, A., and J. Wakefield, 1996: WFO-Advanced: an AWIPS-like prototype forecaster workstation. Preprints, 12th Int. Conf. on Interactive Information and Processing Systems for Meteorology, Oceanography, and Hydrology, Atlanta, GA, Amer. Meteor. Soc., 190-193.

Miller, D. A., and F. Sanders, 1980: Mesoscale conditions for the severe convection of 3 April 1974 in the east-central United States. *J. Atmos. Sci.*, **37,** 1041–1055.

Miller, D., Mann, G. 2010: Observations of Near-Surface Thermodynamic and Wind Shear Profiles on Significant Tornado Days. 18th Annual Great Lakes Operational Meteorology Workshop. Toronto, Ontario Canada, National Weather Service and Environment Canada

Moller A., C. Doswell III, M. Foster, and G. Woodall, 1994: The operational recognition of supercell environments and storm structures, Wea. Forecasting., **9**, 327-347.

Murphy, T.A., K.R. Knupp, 2013: Prevalence and Characteristics of Atmospheric Waves in Severe Weather Environments. Preprints, 94th Annual Conf., Atlanta, GA, Amer. Meteor. Soc.

Murphy, T. A., R. A. Wade, T. A. Coleman, and K. R. Knupp, 2014: Observations and analysis of reflectivity segments interacting with a quasi-linear convective system. Currently in review at Mon. Wea. Rev.

Schmidt, J. M., and W. R. Cotton, 1990: Interactions between upper and lower tropospheric gravity waves on squall line structure and maintenance. *J. Atmos. Sci.*, **47,** 1205–1222.

SPC, cited 2013: Severe Weather Event: Nov 17, 2013. [Available online at http://www.spc.noaa.gov/exper/archive/event.php?date=20131117.]

Stobie, J., F. Einaudi, and L. Uccellini, 1983: A case study of gravity waves–convective storms interaction: 9 May 1979. J. Atmos. Sci., **40**, 2804–2830.

Stobie, J. G., F. Einaudi, and L. W. Uccellini, 1983: A case study of gravity waves–convective storms interaction: 9 May 1979. *J. Atmos. Sci.*, **40,** 2804–2830.

Storm Data, U.S. Dept. of Commerce, 2013: [Available at http://www.ncdc.noaa.gov/].

Uccellini, L. W., 1975: A case study of apparent gravity wave initiation of severe convective storms. *Mon. Wea. Rev.*, **103,** 497–513.